atmosphere

Article

Influence of Various Urban Morphological Parameters on Urban Canopy Ventilation: A Parametric Numerical Study

Liyue Zeng [1,2,3], Xuelin Zhang [1], Jun Lu [4], Yongcai Li [4], Jian Hang [1,2,3], Jiajia Hua [3], Bo Zhao [3] and Hong Ling [1,*]

1 School of Atmospheric Sciences, Sun Yat-sen University, and Southern Marine Science and Engineering Guangdong Laboratory (Zhuhai), Zhuhai 519082, China; zengly29@mail.sysu.edu.cn (L.Z.); zhangxlin25@mail.sysu.edu.cn (X.Z.); hangj3@mail.sysu.edu.cn (J.H.)
2 Key Laboratory of Urban Meteorology, China Meteorological Administration, Beijing 100089, China
3 China Meteorological Administration Xiong'an Atmospheric Boundary Layer Key Laboratory, Xiong'an 071700, China; ustchuajiajia@163.com (J.H.); besz_zb@126.com (B.Z.)
4 School of Civil Engineering, Chongqing University, Chongqing 400045, China; lujun@cqu.edu.cn (J.L.); yongcail85@163.com (Y.L.)
* Correspondence: lingh23@mail.sysu.edu.cn

Abstract: Numerical simulation is vital for evaluating urban ventilation. However, accurate urban-scale ventilation modeling requires extensive building surface simulation for computational demand. The distributed drag force approach simplifies the urban canopy by modeling buildings as a porous volume that accounts for momentum and turbulence. This method is a practical solution for simulating urban airflow. The drag force coefficient (C_d) is a crucial aerodynamic parameter in this approach. This study examines how C_d varies with urban design parameters such as plan area density (λ_p), average building height (H), frontal area density (λ_f), floor aspect ratio (AR), and sky view factor (SVF). Employing extensive numerical simulations conducted under neutral atmospheric conditions, we explore ranges of λ_p = 0.04–0.07 and λ_f = 0.1–1.2. The numerical model has been validated against existing wind tunnel data. The results show that C_d is insensitive to the model scale and background wind speed. We discover a nonlinear relationship between C_d and the parameters λ_p, λ_f, and SVF. For urban layouts with cubic-shaped buildings, C_d peaks at different λ_p within the range of 0.2~0.8. When λ_p and H are constant, C_d has a linear relationship with AR and λ_f. It is recommended to use λ_p, SVF, and AR as predictors for C_d across various urban configurations.

Keywords: urban morphology; urban ventilation; drag force coefficient; parametrical analysis; sky view factor

check for updates

Citation: Zeng, L.; Zhang, X.; Lu, J.; Li, Y.; Hang, J.; Hua, J.; Zhao, B.; Ling, H. Influence of Various Urban Morphological Parameters on Urban Canopy Ventilation: A Parametric Numerical Study. *Atmosphere* **2024**, *15*, 352. https://doi.org/10.3390/atmos15030352

Academic Editor: Martin Piringer

Received: 29 December 2023
Revised: 10 March 2024
Accepted: 11 March 2024
Published: 13 March 2024

1. Introduction

Densely built-up cities suffer from problems such as the accumulation of pollutants from traffic [1], wind discomfort in the pedestrian zones [2], and haze–fog episodes [3,4]. Therefore, it is important to predict, evaluate, and optimize ventilation conditions within the urban canopy. Urban ventilation is a complex phenomenon influenced by the layout and density of buildings and has been the subject of extensive research at scales ranging from individual neighborhoods to entire cities, using experimental, numerical, and analytical methods [5–7].

At building and neighborhood scales, computational fluid dynamics (CFD) can predict detailed wind flow characteristics with highly realistic building shapes [8,9], with the stagnant zones and negative wake flow regions between buildings well resolved. However, the high computational cost of these detailed simulations limits their use at larger scales. To overcome this obstacle, some city-level numerical studies simplify an entire city into basic shapes [10,11], but this can compromise accuracy. A promising alternative that can reduce computational cost is to simplify building clusters as porous control volumes. This method is often referred to as the "macroscopic" method or "distributed drag force" method [11–15], where source terms are added to flow and turbulent models [12,13]. These methods can be divided into two types. One is inspired by the vegetation canopy models, where the drag force is determined by the drag force coefficient C_d and the frontal area density λ_f (hereafter referred to as the $C_d \cdot \lambda_f$ method). C_d can be calculated using the total force acting on the surface and the mean velocity in a control volume. Another method is based on the classical porous media approach, where the source terms consist of the Forchheimer and Darcy terms, which are determined by porosity (the total volume of air in the given volume) and permeability [16]. In both methods, the drag force coefficient C_d is a key parameter describing the influence of obstacles on the flow in the canopy.

Various urban morphological parameters are closely related to C_d, such as the plan area density (λ_p, the percentage of building floor area to the plan area), the frontal area density (λ_f, the percentage of the frontal area of buildings to the plan area) [17–20], the average height of the buildings [21–24], etc. Current knowledge of the relationships between urban morphology and C_d is primarily developed from idealized urban canopy models, in which buildings are simplified as arrays of cubes. These studies have revealed that how spatial parameters affect C_d varies with array configurations [25–28]. For instance, Kanda et al. [25] investigated cube arrays with a plan area density of 0–40% using large eddy simulation (LES) and found that C_d was sensitive to λ_p for staggered arrays but not for square arrays. Hagishima et al. [26] expanded on this by conducting wind tunnel experiments on 63 block arrays with different layouts, wind directions, block heights, and plan area densities. They found that C_d was more sensitive to λ_p and λ_f for staggered arrays than for square arrays. Ahmad Zaki et al. [27] also used wind tunnel tests to introduce variability in building orientation and height for building blocks and found that for arrays with a plan area density of 7.7~48.1%, vertical random arrays showed a consistent increase in C_d with λ_f. However, for horizontally random arrays, the estimated C_d peaked at a certain point. Li et al. [24] further investigated the effects of building shape on C_d peaked by wind tunnel experiments on non-uniform building arrays with different shapes (rectangular and H-shaped), wind directions, plan area densities, and frontal area indices. They found that C_d changed significantly when the building floor shape changed from a rectangle to an H shape.

Most of these studies have considered buildings as blocks with square footprints, and these studies have collectively revealed basic relationships between C_d and spatial parameters. For example, the relationship between C_d and λ_p or λ_f is not simply linear. C_d typically increases λ_p until reaching a plateau at about $\lambda_p = 0.3$ [26,28]. Santiago and Martilli [28] have developed a more complex empirical equation, which relates C_d to λ_p (i.e., $C_d = 3.32\ \lambda_p$ when $\lambda_p \leq 0.29$; and $C_d = 1.85$ when $\lambda_p > 0.29$). This relationship has been used in later studies [29] to perform mesoscale simulations of local wind circulation. However, these correlations have been obtained from small samples, and the relationships between C_d and different spatial parameters (e.g., λ_p and λ_f) are often studied separately. Moreover, it is also necessary to extend the range of λ_p and λ_f values to cover real cities.

This study aims to investigate how the drag force coefficient C_d of idealized urban canopies behaves in a variety of morphological conditions. A parametric analysis is employed focusing on morphological parameters including SVF, λ_p, and λ_f. We conduct an extensive series of three-dimensional Reynolds-averaged Navier–Stokes (RANS) numerical simulations on both cubic and rectangular block arrays with $\lambda_p = 0.04$~0.7 and $\lambda_f = 0.1$~1.2. The findings have the potential to refine the application of the drag force approach in real-world wind environment assessments.

2. Methodology

2.1. RANS Canopy Model with Drag Force Approach

Both the Reynolds-averaged Navier–Stokes (RANS) model and large eddy simulations (LESs) are widely used in CFD simulation for urban micro-climate studies [30–33]. The LES model has pretty good precision in simulating and predicting turbulence [34–36]. However, enormous computational resources are required for the LES model. To save the computational resources, RANS simulation is employed in our study. The standard

k-ε model is employed owing to its astonishing performance in predicting airflow [37–39]. In our previous work, we also evaluated the performance of three turbulence models (i.e., standard k-ε model, RNG k-ε model, and realizable k-ε model) compared to wind tunnel data [40]. The standard k-ε model has the best performance among the tested models, especially within the layer from the surface to the building rooftop (i.e., Height = 1H), where the drag force impacts crucially on the flow.

The urban context is characterized as a homogeneous control volume with regular building blocks and square floors (Figure 1). For this control volume, the drag force and mean flow parameters can be obtained from steady-state RANS simulation, where building surfaces are explicitly resolved in the mesh.

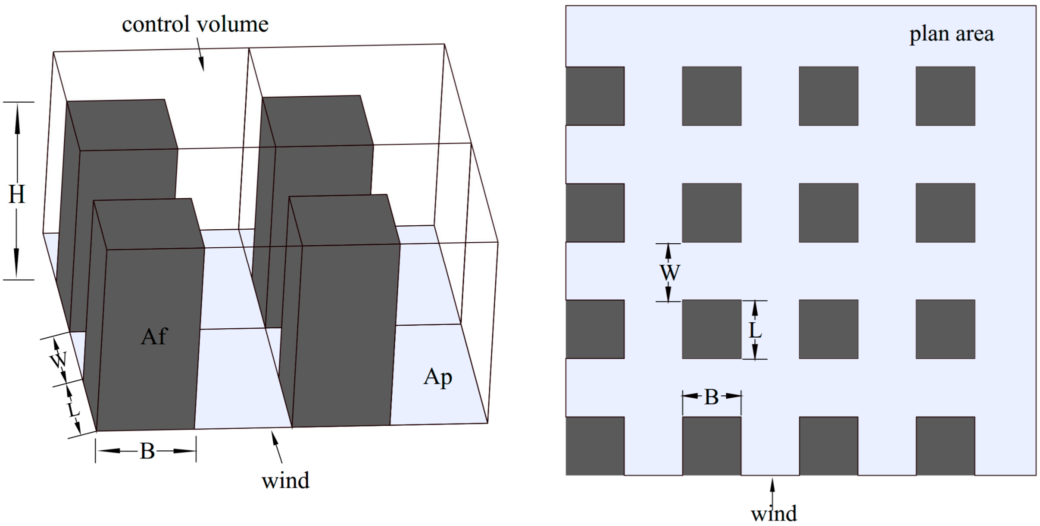

(**a**) (**b**)

Figure 1. Geometric dimensions of building obstacles in the control volume. (**a**) perspective-view model sketch, (**b**) top view of the control volume.

In this study, we conceptualize an idealized urban canopy as a series of regularly aligned rectangular blocks. As an example of a single control volume with four rectangular blocks (Figure 1a), A_p is the total floor area, A_f is the frontal area of all buildings, H is the average height of the blocks, B is the width of block floor facing the wind, L is the length of block floor along the wind direction, and W is the street width. A_B is the area of each floor, i.e., $A_B = B \times L$. The plan area density λ_p can be calculated using Equation (1):

$$\lambda_p = A_B/A_p = B \times L/(B+W)/(L+W) \tag{1}$$

Frontal area density λ_f can be calculated with the following equation:

$$\lambda_f = A_f/A_p = B \times H/(B+W)/(L+W) \tag{2}$$

Frontal area per unit volume A_i, i.e., projected area normal to the *ith* direction per unit volume of the control volume can be calculated with the following equation:

$$A_i = A_f/(A_p \times H) = B/(B+W)/(L+W) \tag{3}$$

The porosity ϕ of the control volume can be calculated as follows:

$$\phi = 1 - \lambda_p \tag{4}$$

The drag force acting on buildings (rectangular block arrays) can be represented by source terms added to the mean momentum equations, where the total drag force term S_i in the *ith* direction can be calculated using Equation (5) [12,14]:

$$S_i = -\rho C_d A_i u_i U S_i = -\rho C_d A_i u_i U, \tag{5}$$

where U is the velocity magnitude and u_i is the velocity component in the *ith* direction. C_d is the drag force coefficient. A_i is not dimensionless, and its value changes with the scale of the model: the models with smaller dimensions have larger A_i. In contrast, for studies using the distributed drag force approach, A_i often refers to the total projected surface area of all buildings facing the wind within the control volume [41]. In this study, the definition of A_i follows the latter definition. The definitions of λ_f vary across studies with different grid sizes. For example, in [18,19], the total projected frontal areas of the first-row buildings within a 100 m by 100 m area have been considered as λ_f.

Equations (6) and (7) are listed as follows for further application of the drag force coefficient C_d if it is required. S_k and S_ε are source terms added to RANS k-ε equations. They represent the production and destruction of turbulence resulting from building obstruction.

$$S_k = \rho C_d A_f \left[\beta_p U^3 - \beta_d U k\right] \tag{6}$$

$$S_\varepsilon = \rho C_d \left[C_{\varepsilon 4} \beta_p \frac{\varepsilon}{k} U^3 - C_{\varepsilon 5} \beta_d U \varepsilon\right] \tag{7}$$

A_f is the total volumetric frontal area of all the blocks within the control volume. B_p is the fraction of mean airflow kinetic energy lost by drag that is converted into turbulent kinetic energy. B_d is the dimensionless coefficient for the short-circulating turbulence cascade [42]. $C_{\varepsilon 4}$ and $C_{\varepsilon 5}$ are dimensionless coefficients. In this model, the drag terms play a similar role to the Forchheimer–Darcy terms (see [16] for detailed information), which also represent the turbulent kinetic energy loss due to form drag. The coefficient group (β_p, β_d, $C_{\varepsilon 4}$, $C_{\varepsilon 5}$) for the sources in the urban canopy model is still a controversial topic in the published literature. Available values for the coefficient group can be as follows: (β_p, β_d, $C_{\varepsilon 4}$, $C_{\varepsilon 5}$) = [(1, 4, 1.5, 1.5), (1, 4, 1.5, 0.6), (1, 5.1, 0.9, 0.9)] [43] for the researchers who are interested in the four coefficients. However, we will not discuss these four coefficients in this paper since this work focuses on how to calculate C_d and how C_d varies with the influence of key factors.

In some drag force approach studies, C_d is obtained at different heights by dividing the whole control volume into various layers of thin slabs [28,44,45]. In this paper, C_d refers to the bulk drag coefficient of the control volume obtained with total drag force and mean flow velocity and can be calculated with Equation (8), where F_i is the total drag force exerted on the building surfaces in the *ith* direction, $\overline{v}$ is the average velocity magnitude of the bulk control volume on the *ith* direction, and A_i is the frontal area per unit volume of buildings projecting to the *ith* direction.

$$C_d = \frac{F_i}{0.5\rho\overline{v}^2 A_i} C_d = \frac{F_i}{0.5\rho\overline{v}^2 A_i} \tag{8}$$

The drag force coefficient C_d is traditionally defined in the literature, particularly in experimental studies, as the ratio of the total surface shear stress τ_0 to the kinetic energy of the fluid, which is related to the free stream wind velocity U_{ref}. This is represented mathematically as $C_d = \tau_0 / 0.5\rho \cdot U_{ref}$ [7,26], where ρ is the fluid density. However, the specific definition of C_d can vary depending on the aims of each study. In our study, we aim to understand how C_d varies in a way that can be applied to the drag force approach in macroscopic CFD simulations; the mean streamwise velocity is therefore used to calculate C_d.

2.2. Idealized Building Array Configurations

We conduct RANS simulations using the standard k-ε model to explore how urban canopy layout affects the drag force coefficient C_d. Two sets of spatial configurations have been investigated and the details are listed in Tables 1 and 2. The geometric dimensions follow the illustrations in Figure 1.

Table 1. Groups of rectangular block arrangements to test the response of C_d to λ_p, λ_f, and *SVF*.

Set	λ_p	$B = L$ (m)	W (m)	H (m)	λ_f	*SVF*	Set	λ_p	$B = L$ (m)	W (m)	H (m)	λ_f	*SVF*
1	0.04	5	20	5	0.05	0.70	6	0.44	40	20	28	0.31	0.30
	0.04	5	20	10	0.10	0.70		0.44	40	20	30	0.33	0.28
	0.04	5	20	20	0.20	0.57		0.44	40	20	40	0.44	0.22
	0.04	5	20	30	0.31	0.49		0.44	40	20	50	0.56	0.19
2	0.08	8	20	8	0.08	0.69		0.44	40	20	63	0.70	0.15
	0.08	8	20	20	0.20	0.51		0.44	40	20	72	0.80	0.14
	0.08	8	20	30	0.31	0.41		0.44	40	20	90	1.00	0.11
3	0.16	20	30	10	0.08	0.66	7	0.51	50	20	10	0.10	0.52
	0.16	20	30	20	0.16	0.52		0.51	50	20	20	0.20	0.36
	0.16	20	30	30	0.24	0.43		0.51	50	20	30	0.31	0.27
	0.16	20	30	40	0.32	0.37		0.51	50	20	40	0.41	0.21
	0.16	20	30	50	0.40	0.32		0.51	50	20	50	0.51	0.18
	0.16	20	30	75	0.60	0.24		0.51	50	20	78	0.80	0.12
	0.16	20	30	100	0.80	0.19		0.51	50	20	98	1.00	0.10
	0.16	20	30	125	1.00	0.16	8	0.58	63.8	20	20	0.18	0.35
4	0.25	20	20	5	0.06	0.70		0.58	63.8	20	40	0.36	0.21
	0.25	20	20	10	0.13	0.57		0.58	63.8	20	64	0.58	0.14
	0.25	20	20	20	0.25	0.40		0.58	63.8	20	80	0.73	0.12
	0.25	20	20	30	0.38	0.31		0.58	63.8	20	100	0.91	0.10
	0.25	20	20	40	0.50	0.25		0.58	63.8	20	120	1.09	0.08
	0.25	20	20	50	0.63	0.21	9	0.65	83.2	20	120	0.94	0.08
	0.25	20	20	64	0.80	0.17		0.65	83.2	20	100	0.78	0.10
	0.25	20	20	80	1.00	0.14		0.65	83.2	20	83	0.65	0.11
	0.25	20	20	96	1.20	0.12		0.65	83.2	20	60	0.47	0.15
5	0.35	29	20	10	0.12	0.54		0.65	83.2	20	40	0.31	0.21
	0.35	29	20	20	0.24	0.38		0.65	83.2	20	30	0.23	0.27
	0.35	29	20	29	0.35	0.30	10	0.7	102.4	20	20	0.14	0.35
	0.35	29	20	40	0.48	0.24		0.7	102.4	20	30	0.21	0.26
	0.35	29	20	50	0.60	0.20		0.7	102.4	20	40	0.27	0.21
	0.35	29	20	66	0.80	0.16		0.7	102.4	20	50	0.34	0.17
	0.35	29	20	83	1.00	0.13		0.7	102.4	20	70	0.48	0.13
	0.35	29	20	100	1.21	0.11		0.7	102.4	20	102.4	0.70	0.09
6	0.44	40	20	10	0.11	0.52		0.7	102.4	20	120	0.82	0.08
	0.44	40	20	20	0.22	0.37		0.7	102.4	20	140	0.96	0.07

Table 2. Groups of rectangular block arrangements to test the response of C_d to floor aspect ratio (for each group: B/L = 0.25, 0.5, 0.75, 1, 2, 3, 4).

Set	1	2	3	4	5	6	7
λ_p	0.16	0.25	0.35	0.44	0.44	0.51	0.58
W (m)	30	20	30	20	20	20	20
H (m)	10	30	66	28	50	20	40

The spatial configurations in Table 1 focus on the impact of plan area density λ_p, frontal area density λ_f, and sky view factor *SVF* on C_d. The building floor is considered to be square ($B = L$). The average building height (H) is in the range of 5–125 m to ensure that λ_f is in the range of 0.05–1.21. The street width is assumed to be fixed at 20 m or 30 m. The largest λ_p is limited to no more than 0.7, allowing for a minimum green coverage ratio (GCR) of 30%.

The second group In Table 2 focuses on the response of C_d to changing floor aspect ratio $AR = B/L$. This is necessary because real urban environments often feature buildings with rectangular floors. In this case, λ_f can be changed due to the stretch of the projected frontal plane in both the vertical and the horizontal direction. To reduce sample size and simulation time, 7 combinations of λ_p and building heights are designed.

2.3. Numerical Settings

For each RANS simulation, a symmetric model is developed with several rows of building blocks repeated along with the flow direction, as shown in Figure 2a. The number of building rows is set to 14 to ensure a fully developed flow. However, in the validation study described in the following section, the number of rows is set to 7, being consistent with the wind tunnel study [46].

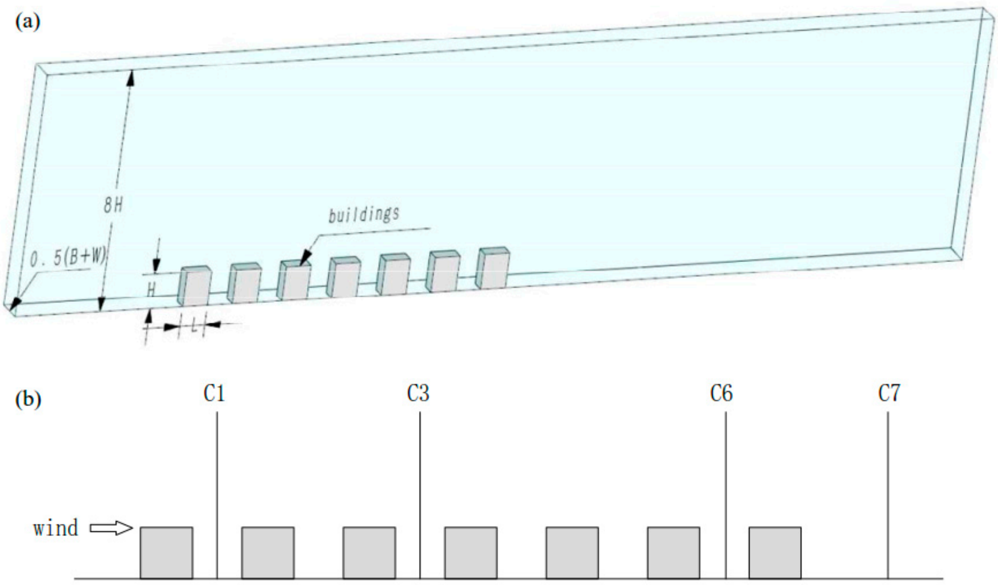

Figure 2. (**a**) Vertical cross-section in the domain of the canopy model for RANS simulation (14 rows) and wind tunnel experiment (7 rows). (**b**) The positions of vertical profiles of streamwise velocity in 4 canyons on the leeward side of the 1st, 3rd, 6th, and 7th obstacles. The profiles obtained at the same positions of the wind tunnel experiments are used for validation study.

The numerical calculations are performed in Ansys Fluent. The boundary condition of the streamwise velocity for the domain inlet is provided by Equations (9)–(11) [46], where $C\mu$ is 0.09, U_H is 3.0 m/s, $u_* = 0.24$ m/s, k_v is von Karman's constant, and the value is 0.41 in this work.

$$U(z) = U_H(z/H)^{0.16} \tag{9}$$

$$k(z) = {u_*}^2/\sqrt{C_\mu} \tag{10}$$

$$\varepsilon(z) = C_\mu^{3/4} k(z)^{3/2}/k_v z \tag{11}$$

Standard wall functions are used for the ground, building walls, and roofs. Zero-gradient boundary conditions are used at the domain outlet and the domain top. The simulations were carried out using the pressure-based model. A second-order upwind discretization scheme was used to solve the momentum and turbulence equations. The PRESTO scheme was used for the pressure correction equation, and the SIMPLE algorithm was used for the pressure–velocity coupling. The convergence criteria for the scaled residuals were set as 10^{-4} for continuity, momentum, and turbulent equations. The geometry of the computational domain is extended to 8*H* in height, 8*H* in the windward direction, and 20*H* in the leeward direction.

2.4. Validation Study

The validation model geometry (Figure 2a) follows the wind tunnel experiment by Lien et al. [46] with λ_p = 0.25. There are 7 rows of buildings, and the dimension of each cubic block is $H = W = B = 0.15$ m. The computational domain is 8*H* high in the vertical direction (z), 6.6*H* long in the streamwise direction (x), and 1*H* wide in the lateral direction (y) in the 3D model. The vertical profiles of streamwise velocity obtained from numerical simulations at the midpoints of 4 canyons (Figure 2b) on the leeward side of the 1st, 3rd, 6th, and 7th obstacles are compared to wind tunnel experiment results. The computation employs a structured grid, and to test the sensitivity of the numerical results to mesh size, we have compared 2 mesh sizes: a fine grid contains 962,444 cells (total grid numbers in x-, y-, and z-directions are 449, 28, and 81, respectively), while a coarse grid contains 684,860 cells (total grid numbers in x-, y-, and z-directions are 446, 22, and 73, respectively).

Figure 3 illustrates that the differences in results from the fine and coarse grid simulations are minimal, particularly within the canopy area. Important statistics for the simulation results of coarse and fine grids are also summarized in Figure 3, including the root mean square error (*RMSE*) and correlation coefficient (R^2). The definitions of *RMSE* and R^2 are shown as Equations (12) and (13), where n is the number of data points; $e_i = S_i - O_i$; and S_i and O_i are simulated and observed values. The results show that the streamwise velocity (*U*) is nearly consistent across both grid sizes, indicating low grid sensitivity for the two sets of grids tested. However, some discrepancies occur in the wake region (C7) and just above the roof level. Despite these minor variations, the model well estimates velocities below the rooftop and is suitable for our parametric study.

$$RMSE = \left[n^{-1}\sum_{i=1}^{n}(e_i)^2\right]^{0.5} \tag{12}$$

$$R^2 = \left(\frac{\sum_{i=1}^{n} O_i S_i - \frac{\sum_{i=1}^{n} O_i \sum_{i=1}^{n} S_i}{n}}{\sqrt{\left[\sum_{i=1}^{n} O_i^2 - \frac{\left(\sum_{i=1}^{n} O_i\right)^2}{n}\right]\left[\sum_{i=1}^{n} S_i^2 - \frac{\left(\sum_{i=1}^{n} S_i\right)^2}{n}\right]}}\right)^2 \tag{13}$$

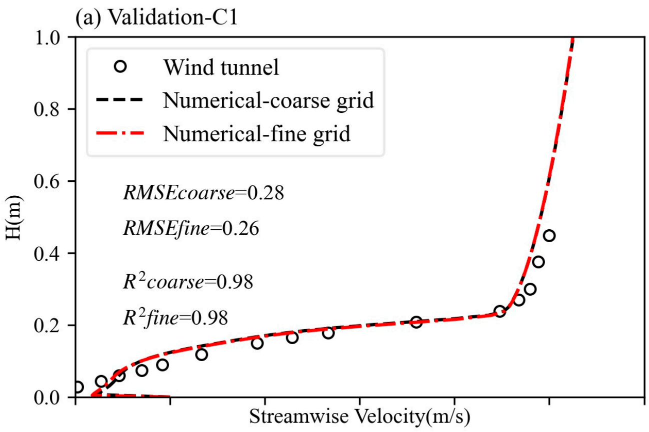

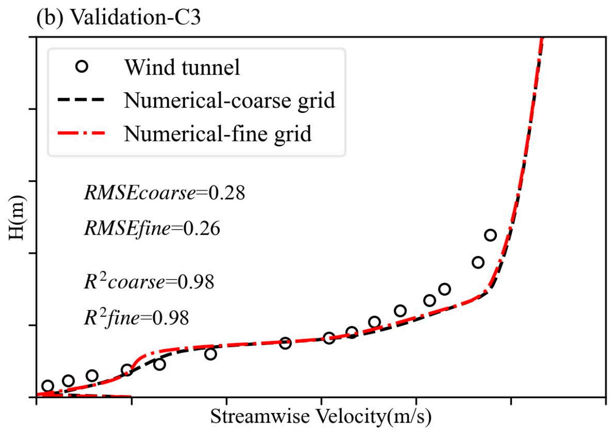

Figure 3. *Cont.*

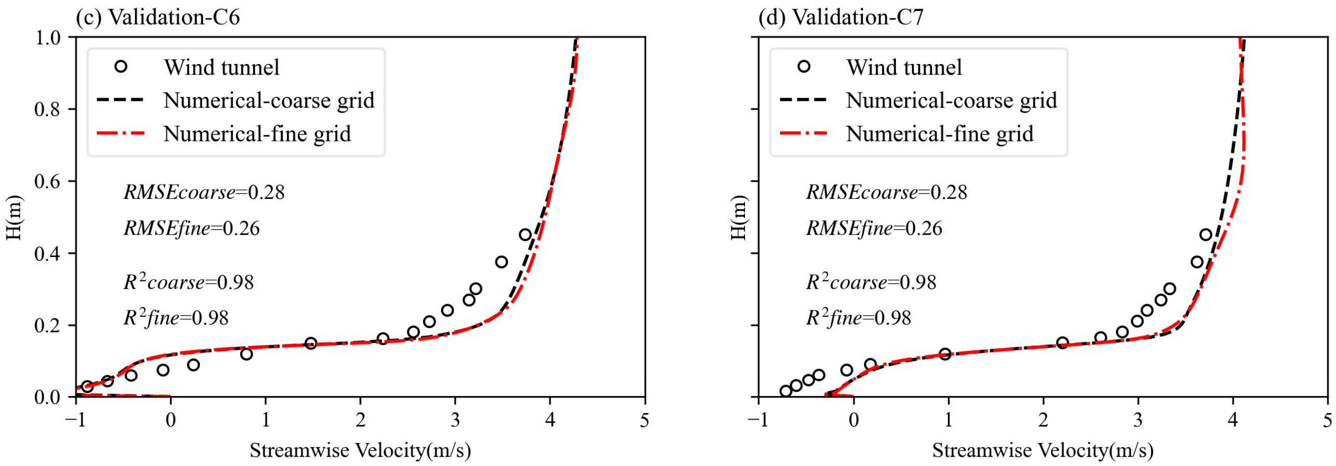

Figure 3. Vertical profiles of streamwise velocity at 4 points from wind-tunnel data and numerical predictions. Subplots (**a**–**d**) are the profiles obtained at the location C1, C3, C6, C7, respectively.

2.5. Effect of Model Scale and Background Wind Condition

Understanding how the drag coefficient (C_d) varies with the model scale is the precondition of utilizing the drag force approach in wind assessment. Existing parameterization studies on C_d for building arrays tend to use reduced scale models in scales of centimeters and millimeters in wind tunnel and numerical studies. This study examines C_d across different scales (centimeters, decimeters, and meters) for three urban canopy types: low-rise low-density (H = 10 m, λ_p = 0.25), mid-rise high-density (H = 28 m, λ_p = 0.44), and high-rise high-density (H = 63 m, λ_p = 0.44). Figure 4a shows the C_d values for these scenarios, demonstrating that the scale of the model does not significantly affect C_d when morphological parameters are constant. This finding suggests that models with different reduced scales or full scales can use the same C_d value without introducing substantial errors. Subsequent sections of this paper will discuss parametric analyses conducted using full-scale numerical models.

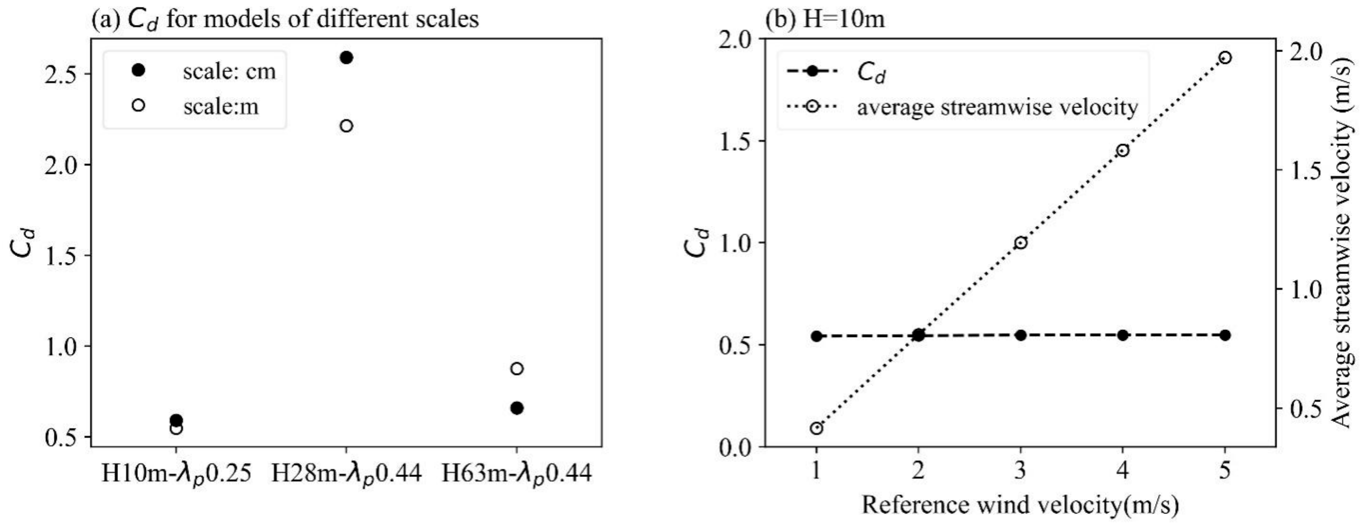

Figure 4. *Cont.*

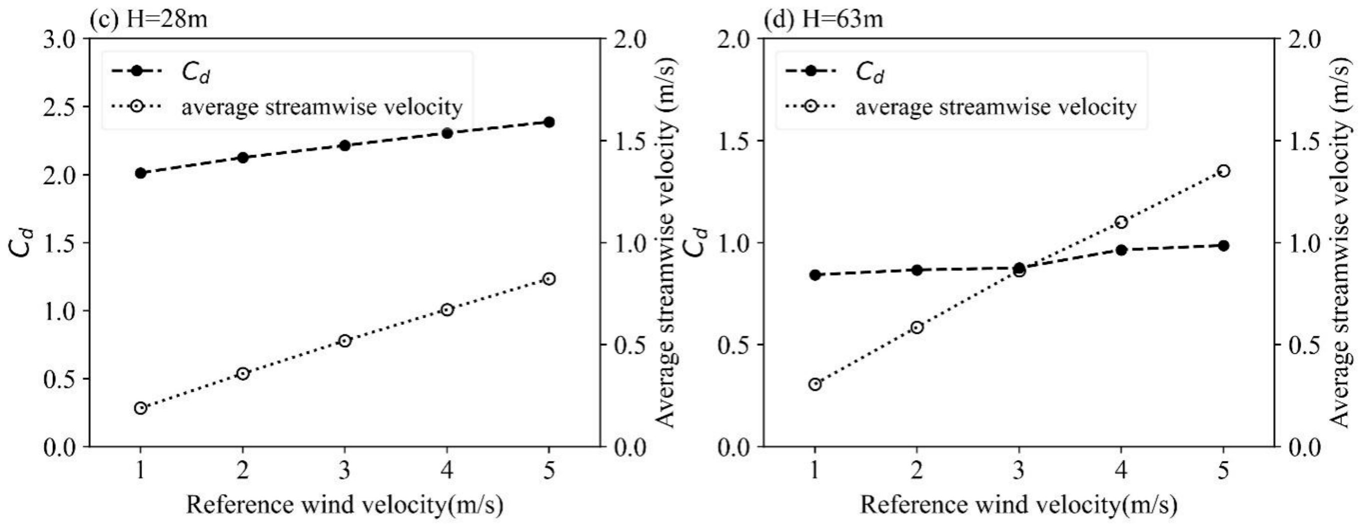

Figure 4. (**a**) Drag force coefficient (C_d) values across different model scales, from full size to wind tunnel scale, and variations of C_d under varying background wind speed (1–5 m/s at 15 m height) and building height: (**b**) H = 10 m, (**c**) H = 28 m, and (**d**) H = 63 m.

The drag force coefficient C_d has also been compared across varying background wind speeds (1–5 m/s at 15 m height), as depicted in Figure 4b–d. The results show that the changes in C_d across different background wind speeds are small for cases with H = 10 m, λ_p = 0.25 and H = 63 m, λ_p = 0.44. For the mid-rise, high-density case (H = 28 m, λ_p = 0.44), where the value of C_d is comparably higher than the other two cases, there is a marginal increase in C_d with higher wind velocities, though the overall variation remains below 0.3. Therefore, we assume that C_d is insensitive to background wind velocity magnitude, and the values of C_d can thus be conveniently applied in practical wind assessment. On the other hand, though with the same λ_p, the value of C_d for the mid-rise canopy (H = 28 m, λ_p = 0.44) is almost double that of the high-rise canopy (H = 63 m, λ_p = 0.44), indicating that the momentum loss of wind speed per unit volume of the mid-rise dense canopy is larger. This contradicts the intuition that a high-rise cluster would result in greater momentum loss of wind.

3. Results and Discussion

3.1. Influence of Urban Morphology on Urban Ventilation in Rectangular Building Blocks

3.1.1. Influence of Urban Morphology on Surface Drag Force and Streamwise Velocity

The total drag force in the control volume is directly related to the drag force coefficient C_d, a key non-dimensional parameter that influences the total surface shear stress and reference flow speed in the urban canopy, as described in the previous section. Figure 5a shows a positive linear relationship between the total drag per unit plan area and the frontal area density (λ_f), with a consistent rate of increase across different plan area densities (λ_p). This is in line with previous studies that reported an increase in C_d with the increase in λ_f [24,26]. However, it may appear counterintuitive that canopies with $\lambda_p \leq 0.35$ experience a higher total drag per unit plan area than those with increased λ_p.

For the mean streamwise wind velocity, Figure 5b depicts its variation with λ_f and λ_p. The results reveal a V-shaped curve for the relationship between streamwise wind velocity and λ_f. The lowest streamwise wind velocity appears at an approximate λ_f of 0.3–0.4, being consistent across all the examined λ_p ranges. Furthermore, Figure 6 shows the spatial mean of the intra-canopy streamwise velocity (denoted as <u_z>) at different heights for different λ_p and building heights. The <u_z> at each height is obtained by averaging streamwise velocity at all the air cells in the control volume at the same height. The <u_z> value consistently rises with height until it reaches a threshold for most canopies.

However, <u_z> in some canopies with higher heights (H = 75 m, 83 m, 100 m) and smaller λ_p (λ_p = 0.16, 0.35) has a distinctive S-shaped curve, which has two inflection points.

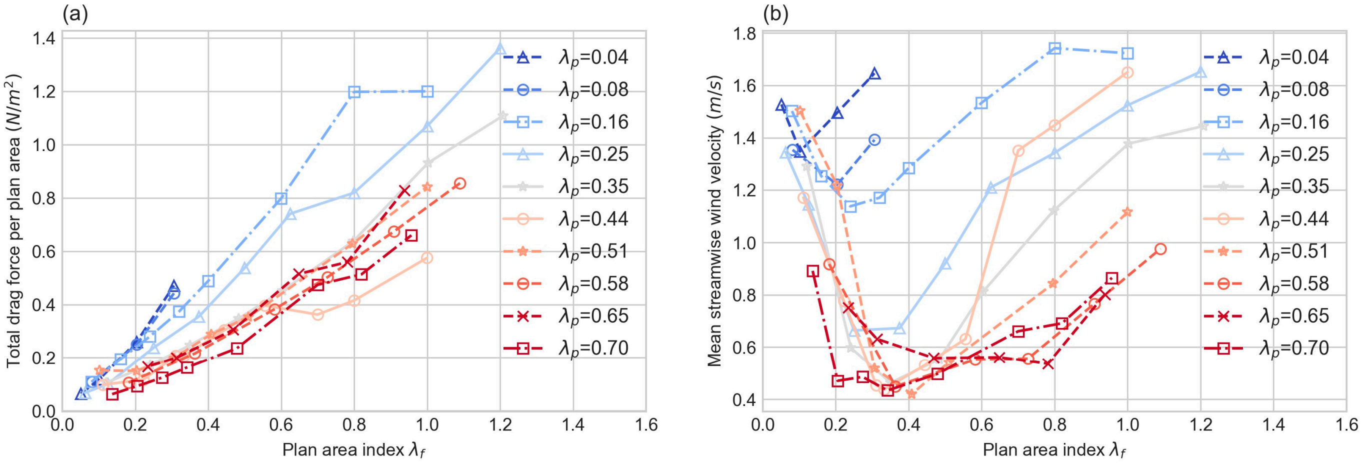

Figure 5. (**a**) Total drag force per unit plan area with different λ_p, (**b**) mean streamwise wind velocity per unit plan area with different λ_p.

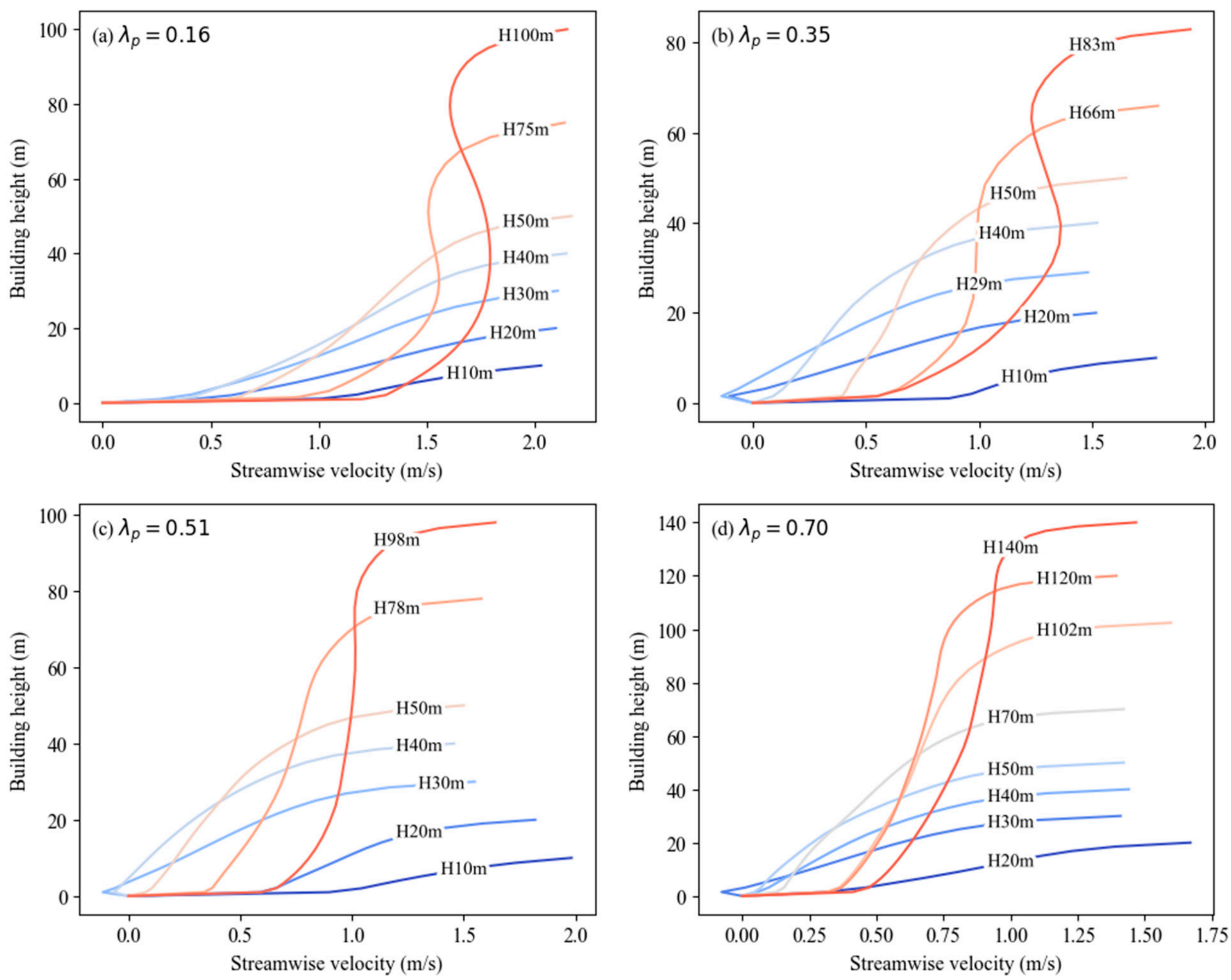

Figure 6. Vertical distribution of streamwise velocity in different canopies with various λ_p: (**a**) λ_p = 0.16; (**b**) λ_p = 0.35; (**c**) λ_p = 0.51; (**d**) λ_p = 0.70.

The above results suggest that the total drag force per unit area is more sensitive to λ_f than to λ_p. Though the drag force per unit area linearly increases with λ_f for any given λ_p, this does not imply a direct negative impact on ventilation performance. From the point of view of the city scale, the intra-canopy wind velocity directly reflects the average ventilation performance of one district, while the total drag force denotes the momentum loss of approaching wind at this control volume and directly affects its leeward control volume. Therefore, a medium λ_f (i.e., λ_f = 0.4 in our study) results in lower drag force, yet it can also lead to reduced wind velocity and poorer ventilation compared to a higher λ_f. Conversely, a high λ_f could cause greater momentum loss and subsequently degrade ventilation in downwind areas. It is the combined effect of both the drag force and the wind velocity in all control volumes of an urban canopy that controls the overall ventilation performance. In other words, the drag force coefficient C_d that developed from both drag force and intra-canopy velocity can be a better choice to denote ventilation performance.

3.1.2. Influence of Urban Morphology on Drag Force Coefficient C_d

With the first set in Table 1, we begin our analysis by considering a widely used assumption in similar studies: $\lambda_p = \lambda_f$ and $B = L = H$, i.e., where the building block is cubic with equal dimensions for breadth (B), length (L), and height (H) and where the plan area index (λ_p) equals the frontal area density (λ_f) [7,28].

Figure 7a illustrates how the drag coefficient C_d is influenced by λ_p, λ_f, and *SVF*. C_d initially increases with λ_p before reaching a peak at approximately λ_p = 0.35, then undergoes a gradual decline, except when λ_p = 0.65. Notably, the decrease in C_d is more gradual compared to its increase. For a small λ_p (λ_p = 0.16), changes in C_d are minimal. However, for higher λ_p, the obstacles within the control volume increase with the increasing λ_p, and the momentum loss of wind increases. Owing to the wake interference flow or skimming flow regime, the obstruction of downstream buildings is weakened because of sheltering. This suggests a transition in flow characteristics within the canopy—from isolated flow with lower λ_p to wake interference or skimming flow with higher λ_p, where downstream building obstruction is reduced due to sheltering effects [47,48]. Our findings are closely aligned with those of Santiago et al. [28], who performed a parametric analysis on the variation in C_d using a uniform staggered array of cubes (where $\lambda_p = \lambda_f$) and derived an empirical equation (Equation (14)). The trend of C_d for λ_f values below 0.44 reported by Santiago et al. [28] is similar to our results. However, an intriguing behavior is noted where C_d noticeably decreases once λ_f surpasses 0.44.

$$C_d = \begin{cases} 3.32\lambda_p & \lambda_p \leq 0.29 \\ 1.85 & \lambda_p > 0.29 \end{cases} \tag{14}$$

Figure 7b shows the variation in $C_d{\cdot}\lambda_f/H$ with λ_f; the trend is similar to that of C_d. The maximum value of $C_d{\cdot}\lambda_f/H$ appears at approximately λ_f = 0.25–0.4. Similar to C_d, the physical meaning of $C_d{\cdot}\lambda_f/H$ is also clear: it represents the obstruction per unit volume of the urban canopy that induces momentum loss in the approaching wind. $C_d{\cdot}\lambda_f$ (Figure 7c) represents the obstruction per unit plan area of the urban canopy acting on the approaching wind, and it increases monotonously with the increase in λ_p. The trend is different from what is revealed for C_d and $C_d{\cdot}\lambda_f\ /H$. For lower λ_p (0–0.51), $C_d{\cdot}\lambda_f$ peaks at where λ_f is around 0.35, while for higher λ_p (0.58–0.7), $C_d{\cdot}\lambda_f$ peaks at where λ_f is around 0.8.

The results show that the effect of *SVF* on parameters C_d, $C_d{\cdot}\lambda_f/H$, and $C_d{\cdot}\lambda$ (Figure 7d–f) shares both similarities and differences with the effect of λ_f. Across all cases in this study, we found that C_d is more likely to reach higher values when *SVF* is between 0.2 and 0.3, not at its lowest when the building clusters show the strongest sheltering effect. This observation diverges from the intuitive expectation that the maximum drag coefficient would coincide with the minimum openness. Particularly, in a densely populated urban area with λ_p of over 0.65, the peak value of C_d and $C_d{\cdot}\lambda_f/H$ is observed when *SVF* is approximately 0.1. Moreover, the relationship between *SVF* and C_d across varying λ_p values demonstrates a non-linear pattern: as *SVF* increases, C_d initially rises and then decreases. This trend suggests an SVF range where the drag coefficient is maximized, beyond which further increases in SVF lead to reductions in C_d. Furthermore, the underlying dynamics between SVF and λ_f (Figure 8) can help to understand this relationship. A relatively regular pattern is observed where an increase in λ_f leads to a decrease in SVF. This inverse relationship between SVF and λ_f makes the effect of SVF on parameters C_d, $C_d{\cdot}\lambda_f/H$, and $C_d{\cdot}\lambda$ simpler to explain: in general, the smaller the SVF, the larger the parameters related to resistance.

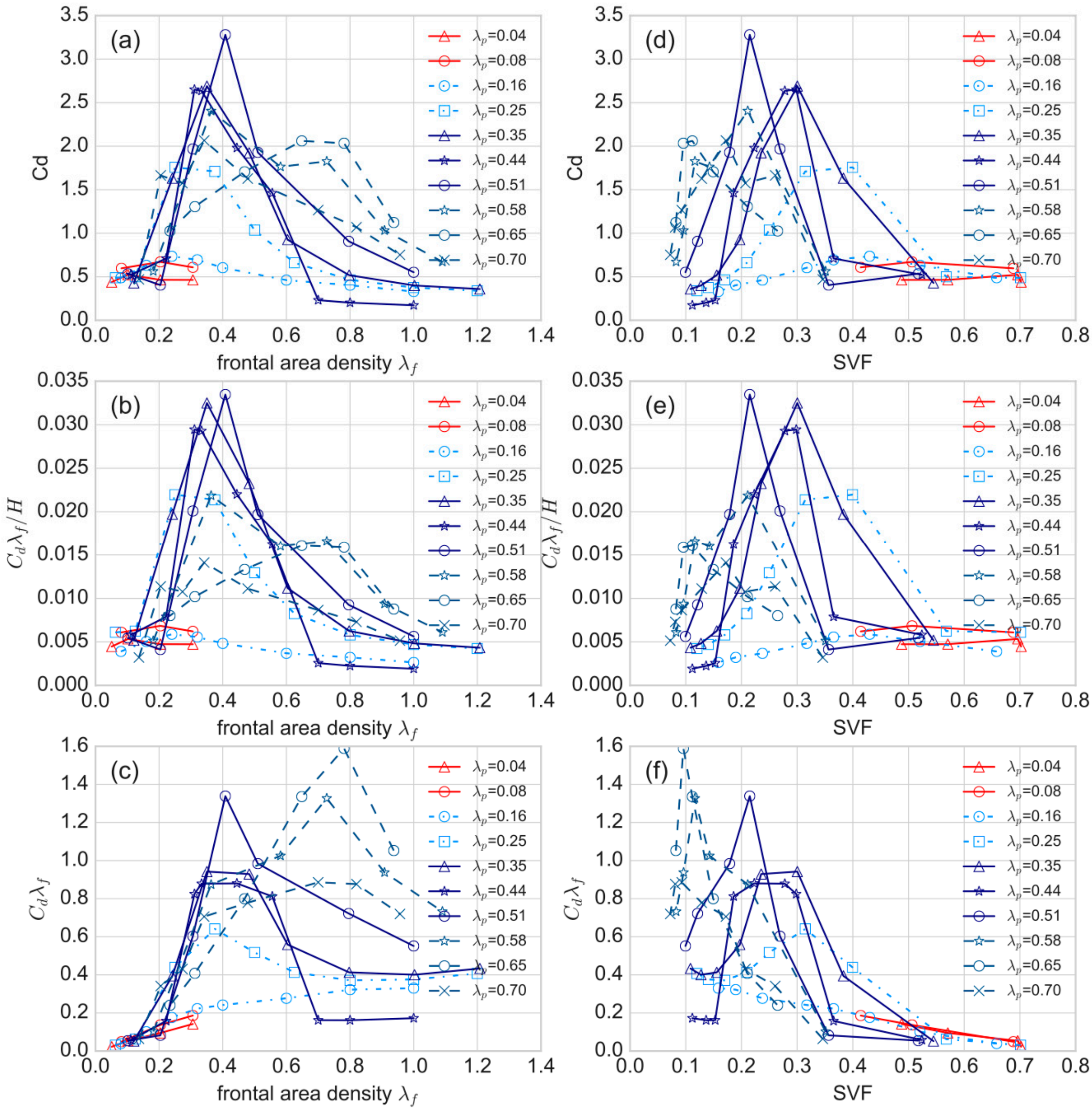

Figure 7. (**a**–**c**) Variation in C_d, $C_d{\cdot}\lambda_f/H$, $C_d{\cdot}\lambda_f$ with λ_f (for λ_p = 0.04~0.7); (**d**–**f**) Variation in C_d, $C_d{\cdot}\lambda_f/H$, $C_d{\cdot}\lambda_f$ with SVF (for λ_p = 0.04~0.7).

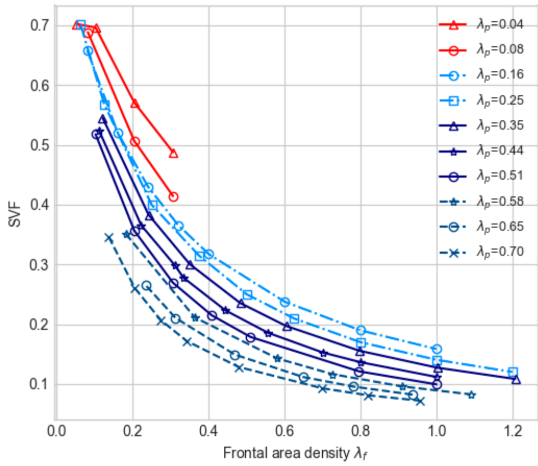

Figure 8. Variation in *SVF* with λ_f across all cases in Table 1.

The choice between using $C_d \cdot \lambda_f / H$ or $C_d \cdot \lambda_f$ as the indicator to describe the impact of turbulence on urban wind optimization depends on the optimization methodology employed. For example, for a GIS-based least-cost-path method (similar to that in [49]) that divides the city into a grid of patches, $C_d \cdot \lambda_f$ could be a more acceptable indicator since it directly implies the total momentum loss of wind on each grid. If only the lower level of the canopy (below the roof of mid-rise building clusters) is the optimized target, $C_d \cdot \lambda_f / H$ could also be a favorable indicator. Though current evidence is still insufficient to determine which one of the two indicators is superior, both of them are promising alternatives for the commonly used parameter λ_f.

Figure 9a–c illustrate the interpolation results of C_d, $C_d \cdot \lambda_f / H$, and $C_d \cdot \lambda_f$ with 2D contour graphs to further reveal the response of these three indicators under the combined effect of λ_p and λ_f. It can be seen that a local maximum of C_d and $C_d \cdot \lambda_f / H$ appears near (λ_p, λ_f) = (0.3~0.5, 0.4). A local maximum of $C_d \cdot \lambda_f$ appears near (λ_p, λ_f) = (0.6, 0.4~0.8). The trend of C_d in our results is almost identical to that of Santiago et al. [28] when λ_p is smaller than 0.44. Interestingly, C_d obviously decreases when λ_p exceeds 0.44. Urban buildings are influenced by their nearest surroundings, but lacking a detailed representation of the area is a huge challenge for accurate ventilation predictions. Figure 9d–f demonstrates how the combination of λ_p and *SVF* influences these resistance-related parameters (C_d, $C_d \cdot \lambda_f / H$, and $C_d \cdot \lambda_f$) through interpolation results. Unlike the effect of λ_f, these resistance parameters show an overall decreasing trend with the increase in *SVF*. The contour plots of C_d in Figure 9 could be used in macroscopic or drag force approach-based numerical simulations that can reduce mesh number and simplify the physical model (refer to [11,15]).

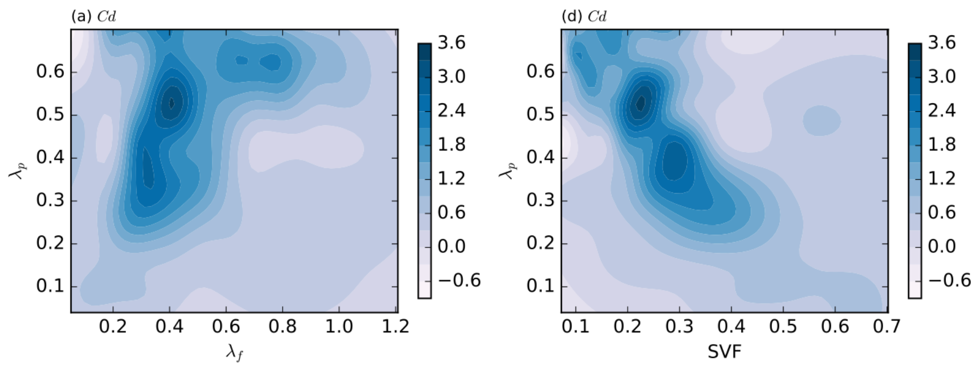

Figure 9. *Cont.*

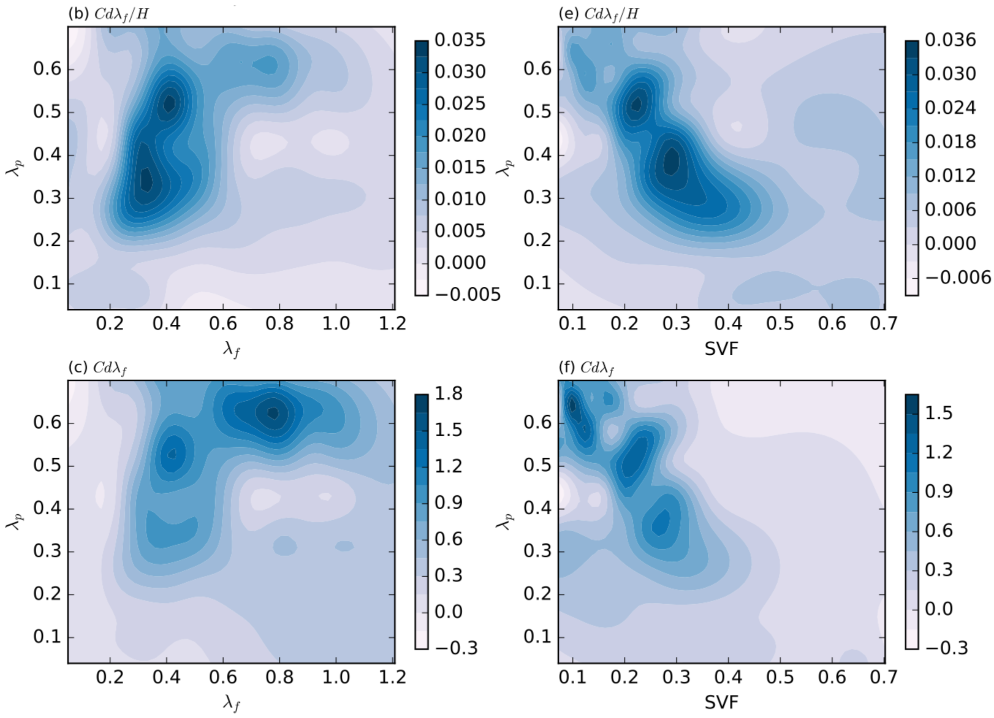

Figure 9. (**a**–**c**) Contours of C_d, $C_d{\cdot}\lambda_f/H$, and $C_d{\cdot}\lambda_f$ with varying λ_p and λ_f; (**d**–**f**) contours of C_d, $C_d{\cdot}\lambda_f/H$, and $C_d{\cdot}\lambda_f$ with varying λ_p and *SVF*.

3.2. Effect of Building Floor AR (Aspect Ratio) on Drag Force Coefficient C_d

Previous sections focused on scenarios when $\lambda_f = \lambda_p$, where λ_f increases with rising building height. However, in real urban areas, λ_f also changes with the aspect ratio (*AR*) of the building floor. This section investigates the variation in C_d with changing building floor *AR*. This group of cases is designed with fixed variables (i.e., canopy height *H*, building plan area density λ_p, and street width *W*) listed in Table 2. Figure 10 illustrates that C_d increases linearly with *AR*, and the slope of C_d becomes the largest in canopies with larger λ_p and larger *H* (i.e., λ_p = 0.44, *H* = 50 m; and λ_p = 0.58, *H* = 40 m).

These results suggest that the aspect ratio of the building floor is also a significant factor that affects C_d. Despite having less research interests in GIS-aided urban ventilation studies compared to λ_p and λ_f, the significance of building floor *AR* requires more attention.

λ_f may increase due to taller buildings or larger building floor *AR* in urban planning. For a fixed H/W, a linear increase in C_d with rising λ_f is observed when it is related to floor length. However, C_d initially increases and then decreases with increasing λ_f for taller buildings. Therefore, considering the building floor *AR* reveals that neither λ_f nor λ_p can fully capture the variations in C_d in isolation. As shown in Figure 10, the sky view factor *SVF* changes little with building floor *AR* but is influenced by λ_p and H/W distinctly. This recommends a two-step approach to estimating C_d, starting with λ_p and *SVF* for a rough estimate, then refining it with the floor *AR* for better precision. Based on the above analysis, it is highly recommended to use three parameters (i.e., λ_p, *SVF*, and floor *AR*) to estimate the drag force coefficient C_d for a given urban area. In addition, using λ_p, λ_f, and floor *AR* for C_d estimation is reasonable too. Although the logic between λ_f and C_d still needs comprehensive exploration, it is possible to develop relationships and is easier to obtain frontal area density for practical design activities with the GIS technique.

The question of whether taking urban surfaces as regular geometry is still open, and the effect of spatial inhomogeneity can be a future research direction. A limitation of this macroscopic model is the reliance on a substantial number of obstacles within the representative element volume for accurate predictions. The model precision is reduced in areas with few obstacles or where the airflow is not fully developed.

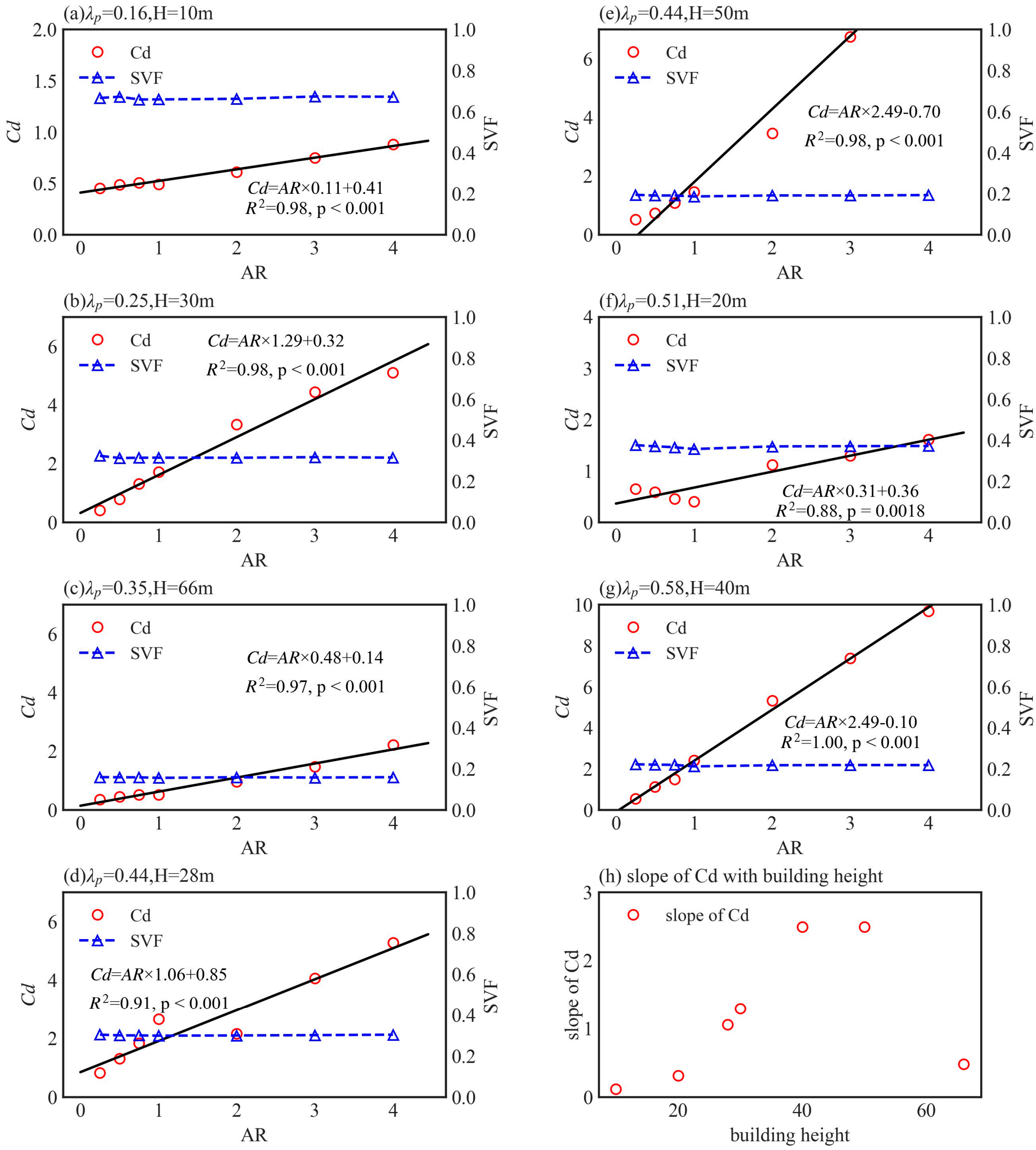

Figure 10. (**a**–**g**) Variation in C_d with *AR* for cases in Table 2; (**h**) variation in the increasing slope of C_d with building height.

3.3. Limitations and Future Work

In this study, we focused on evaluating the impact of various urban design parameters, such as plan area density (λ_p), average building height (H), frontal area density (λ_f), floor aspect ratio (AR), and sky view factor (SVF) on the drag force coefficient (C_d) using numerical simulations under neutral atmospheric conditions. Our research aimed to provide insights into how these parameters influence urban ventilation, leveraging a distributed drag force approach to model buildings as porous volumes. This approach simplifies the complex urban canopy, making it feasible to simulate urban-scale airflow with practical computational demands. The numerical model was validated against existing wind tunnel data, ensuring the reliability of our findings. However, the applicability of the model can be questionable when the airflow is not fully developed.

We also acknowledge that there are additional parameters that could influence C_d, such as building orientation, variability in building height, and the presence of vegetation.

However, introducing these parameters as variables would have significantly increased the complexity of the model and the computational demand. Therefore, the question of whether it is appropriate to take urban surfaces as regular geometry is still open, and the effect of spatial inhomogeneity can be a future research direction. Moreover, different validation studies may be required for studies involving these parameters. Future studies can add more parameters, including those mentioned above, to provide a more comprehensive understanding of urban airflow dynamics.

Furthermore, our simulations have been conducted under neutral atmospheric conditions. Although it does not fully capture the variability introduced by different atmospheric stability conditions, it provides a controlled environment for studying the influence of urban design on airflow. Real-world urban airflow dynamics are influenced by a range of complex atmospheric conditions. Future studies have been planned to explore how varying stability conditions affect the relationship between urban design parameters and C_d using either numerical simulations or scaled outdoor measurements [50–53] that are exposed to varying weather conditions. An observation campaign in the real city is also planned in future work.

4. Conclusions

This study investigates the influences of urban morphology on ventilation, using idealized urban canopy models with square building arrays. We focus on two key parameters, the plan area density (λ_p) and the frontal area density (λ_f), which represent urban density and roughness, respectively. Additionally, the sky view factor (*SVF*) is calculated for each layout. Three-dimensional RANS simulations with varying λ_p and λ_f were conducted with building blocks explicitly resolved inside the canopy model. The numerical model has been validated against wind tunnel results from the published literature. We compute the drag force coefficient C_d (an aerodynamic parameter derived from the total drag and average wind speed) within the urban canopy in these simulations. This coefficient C_d can simplify urban airflow modeling by implicitly considering building surfaces, thus reducing computational demands.

The results show that for a constant λ_p, C_d increases linearly with rising λ_f, with a consistent rate across different λ_p values. Conversely, the average wind speed within the canopy firstly decreases and then increases with increasing λ_f, and the minimum appears at around λ_f = 0.3–0.4. Effective city-scale ventilation depends on the combined impact of these parameters. Since C_d incorporates both drag and intra-canopy wind speed, it can be a promising indicator for urban ventilation assessment.

Furthermore, the generic pattern of drag coefficient C_d is obtained. The response to the combined effects of λ_p, λ_f, and *SVF* is illustrated with a 2D contour graph. A local maximum of C_d and $C_d \cdot \lambda_f / H$ will appear when (λ_p, λ_f) = (0.3~0.5, 0.4), and a local maximum of $C_d \cdot \lambda_f / H$ would appear when (λ_p, λ_f) = (0.6, 0.4~0.8). The variation in C_d with model scale and background wind velocity is insignificant. With the condition of $\lambda_p = \lambda_f$, the estimated C_d peaks at a medium value of λ_p. The changing of C_d with λ_f behaves in different patterns when λ_p varies. When λ_p is small, C_d exhibits little or no sensitivity to changes in λ_f. However, C_d typically peaks around λ_f = 0.3–0.4, except when λ_f is 0.65. Moreover, for a given building height and λ_p, there is a positive linear relationship between C_d and λ_f. It is strongly recommended to use λ_p, *SVF*, and the building floor *AR* as key indicators for characterizing the drag force effect of urban areas.

Compared to parameterizations using length scale and displacement height, the use of drag coefficient (C_d)-related parameters enables assessing of urban scale ventilation with 3D numerical models. Employing C_d-related parameters, as opposed to traditional length scale and displacement height metrics, can improve the assessment of urban-scale ventilation through 3D numerical models with a drag force approach. Utilizing a drag force approach within mesh-reduced numerical methods shows considerable promise for practical evaluations of urban ventilation and air quality. Moreover, the approach and methodology set up in this work have significant implications for the monitoring and modeling research on urban climate, and the application of the method can be extended to the area of human exposure and public health. The application of the methodology and the findings in this work also offer scientific references for sustainable urban planning and strengthen the resilience of urban development.

Author Contributions: Conceptualization, L.Z.; methodology, L.Z., X.Z. and H.L.; software, L.Z., X.Z. and H.L.; validation, X.Z. and H.L.; formal analysis, L.Z.; investigation, L.Z., X.Z. and H.L.; resources, J.H. (Jian Hang), L.Z., Y.L., J.L. and J.H. (Jiajia Hua); data curation, H.L. and L.Z.; writing—original draft preparation, L.Z. and H.L.; writing—review and editing, H.L., L.Z., J.L., Y.L., J.H. (Jian Hang), X.Z., J.H. (Jiajia Hua) and B.Z.; visualization, L.Z.; supervision, H.L. and J.H. (Jian Hang); project administration, H.L. and J.L.; funding acquisition, J.H. (Jian Hang), H.L. and L.Z. All authors have read and agreed to the published version of the manuscript.

Funding: This study is supported by the National Natural Science Foundation of China (Nos. 42105070, 42175094, 42175095 and 41875015), the Guangdong Basic and Applied Basic Research Foundation (No. 2020A1515110278), and the Innovation Group Project of Southern Marine Science and Engineering Guangdong Laboratory (No. 311020001).

Institutional Review Board Statement: Not applicable.

Informed Consent Statement: Not applicable.

Data Availability Statement: Data are contained within the article.

Conflicts of Interest: The authors declare no conflicts of interest.

References

1. Richmond-Bryant, J.; Reff, A. Air pollution retention within a complex of urban street canyons: A two-city comparison. *Atmos. Environ.* **2012**, *49*, 24–32. [CrossRef]
2. Blocken, B.; Carmeliet, J. Pedestrian Wind Environment around Buildings: Literature Review and Practical Examples. *J. Build. Phys.* **2004**, *28*, 107–159. [CrossRef]
3. Zhang, J.; Chen, J.; Yang, L.; Sui, X.; Yao, L.; Zheng, L.; Wen, L.; Xu, C.; Wang, W. Indoor PM2.5 and its chemical composition during a heavy haze-fog episode at Jinan, China. *Atmos. Environ.* **2014**, *99*, 641–649. [CrossRef]
4. Tao, M.; Chen, L.; Xiong, X.; Zhang, M.; Ma, P.; Tao, J.; Wang, Z. Formation process of the widespread extreme haze pollution over northern China in January 2013: Implications for regional air quality and climate. *Atmos. Environ.* **2014**, *98*, 417–425. [CrossRef]
5. Blocken, B. 50 years of Computational Wind Engineering: Past, present and future. *J. Wind Eng. Ind. Aerodyn.* **2014**, *129*, 69–102. [CrossRef]
6. Barlow, J.F. Progress in observing and modelling the urban boundary layer. *Urban Clim.* **2014**, *10*, 216–240. [CrossRef]
7. Cheng, H.; Hayden, P.; Robins, A.G.; Castro, I.P. Flow over cube arrays of different packing densities. *J. Wind Eng. Ind. Aerodyn.* **2007**, *95*, 715–740. [CrossRef]
8. Palusci, O.; Monti, P.; Cecere, C.; Montazeri, H.; Blocken, B. Impact of morphological parameters on urban ventilation in compact cities: The case of the Tuscolano-Don Bosco district in Rome. *Sci. Total Environ.* **2022**, *807*, 150490. [CrossRef]
9. Brozovsky, J.; Simonsen, A.; Gaitani, N. Validation of a CFD model for the evaluation of urban microclimate at high latitudes: A case study in Trondheim, Norway. *Build. Environ.* **2021**, *205*, 108175. [CrossRef]
10. Saitoh, T.S.; Shimada, T.; Hoshi, H. Modeling and simulation of the Tokyo urban heat island. *Atmos. Environ.* **1996**, *30*, 3431–3442. [CrossRef]
11. Hang, J.; Sandberg, M.; Li, Y. Age of air and air exchange efficiency in idealized city models. *Build. Environ.* **2009**, *44*, 1714–1723. [CrossRef]
12. Coceal, O.; Belcher, S.E. A canopy model of mean winds through urban areas. *Q. J. R. Meteorol. Soc.* **2004**, *130*, 1349–1372. [CrossRef]
13. Coceal, O.; Belcher, S.E. Mean winds through an inhomogeneous urban canopy. *Bound.-Layer Meteorol.* **2005**, *115*, 47–68. [CrossRef]
14. Liu, J.; Chen, J.M.; Black, T.A.; Novak, M.D. E-epsilon modelling of turbulent air flow downwind of a model forest edge. *Bound.-Layer Meteorol.* **1996**, *77*, 21–44. [CrossRef]
15. Lien, F.S.; Yee, E.; Cheng, Y. Simulation of mean flow and turbulence over a 2D building array using high-resolution CFD and a distributed drag force approach. *J. Wind Eng. Ind. Aerodyn.* **2004**, *92*, 117–158. [CrossRef]
16. Antohe, B.V.; Lage, J.L. A general two-equation macroscopic turbulence model for incompressible flow in porous media. *Int. J. Heat Mass Transf.* **1997**, *40*, 3013–3024. [CrossRef]
17. Ng, E.; Yuan, C.; Chen, L.; Ren, C.; Fung, J.C.H. Improving the wind environment in high-density cities by understanding urban morphology and surface roughness: A study in Hong Kong. *Landsc. Urban Plan.* **2011**, *101*, 59–74. [CrossRef]

18. Wong, M.S.A.; Nichol, J.E.A.; Ng, E.Y.Y.B.; Guilbert, E.A.; Kwok, K.H.A.; To, P.H.A.; Wang, J.Z.A. GIS techniques for mapping urban ventilation, using frontal area index and least cost path analysis. *Int. Arch. Photogramm. Remote Sens. Spat. Inf. Sci.—ISPRS Arch.* **2010**, *38*, 586–591.
19. Wong, M.S.; Nichol, J.E.; To, P.H.; Wang, J. A simple method for designation of urban ventilation corridors and its application to urban heat island analysis. *Build. Environ.* **2010**, *45*, 1880–1889. [CrossRef]
20. Macdonald, R.W. Modelling the Mean Velocity Profile in the Urban Canopy Layer. *Bound.-Layer Meteorol.* **2000**, *97*, 25–45. [CrossRef]
21. Srebric, J.; Heidarinejad, M.; Liu, J. Building neighborhood emerging properties and their impacts on multi-scale modeling of building energy and airflows. *Build. Environ.* **2015**, *91*, 246–262. [CrossRef]
22. Hang, J.; Li, Y. Macroscopic simulations of turbulent flows through high-rise building arrays using a porous turbulence model. *Build. Environ.* **2012**, *49*, 41–54. [CrossRef]
23. Chen, L.; Hang, J.; Sandberg, M.; Claesson, L.; Di Sabatino, S.; Wigo, H. The impacts of building height variations and building packing densities on flow adjustment and city breathability in idealized urban models. *Build. Environ.* **2017**, *118*, 344–361. [CrossRef]
24. Li, B.; Liu, J.; Li, M. Wind tunnel study on the morphological parameterization of building non-uniformity. *J. Wind Eng. Ind. Aerodyn.* **2013**, *121*, 60–69. [CrossRef]
25. Kanda, M. Large-eddy simulations on the effects of surface geometry of building arrays on turbulent organized structures. *Bound.-Layer Meteorol.* **2006**, *118*, 151–168. [CrossRef]
26. Hagishima, A.; Tanimoto, J.; Nagayama, K.; Meno, S. Aerodynamic parameters of regular arrays of rectangular blocks with various geometries. *Bound.-Layer Meteorol.* **2009**, *132*, 315–337. [CrossRef]
27. Zaki, S.A.; Hagishima, A.; Tanimoto, J.; Ikegaya, N. Aerodynamic Parameters of Urban Building Arrays with Random Geometries. *Bound.-Layer Meteorol.* **2011**, *138*, 99–120. [CrossRef]
28. Santiago, J.L.; Martilli, A. A Dynamic Urban Canopy Parameterization for Mesoscale Models Based on Computational Fluid Dynamics Reynolds-Averaged Navier-Stokes Microscale Simulations. *Bound.-Layer Meteorol.* **2010**, *137*, 417–439. [CrossRef]
29. Gutiérrez, E.; Martilli, A.; Santiago, J.L.; González, J.E. A Mechanical Drag Coefficient Formulation and Urban Canopy Parameter Assimilation Technique for Complex Urban Environments. *Bound.-Layer Meteorol.* **2015**, *157*, 333–341. [CrossRef]
30. Blocken, B. Computational Fluid Dynamics for urban physics: Importance, scales, possibilities, limitations and ten tips and tricks towards accurate and reliable simulations. *Build. Environ.* **2015**, *91*, 219–245. [CrossRef]
31. Gao, Z.L.; Bresson, R.; Qu, Y.F.; Milliez, M.; de Munck, C.; Carissimo, B. High resolution unsteady RANS simulation of wind, thermal effects and pollution dispersion for studying urban renewal scenarios in a neighborhood of Toulouse. *Urban Clim.* **2018**, *23*, 114–130. [CrossRef]
32. Li, X.-X.; Britter, R.E.; Norford, L.K. Transport processes in and above two-dimensional urban street canyons under different stratification conditions: Results from numerical simulation. *Environ. Fluid Mech.* **2015**, *15*, 399–417. [CrossRef]
33. Wang, W.; Ng, E. Air ventilation assessment under unstable atmospheric stratification—A comparative study for Hong Kong. *Build. Environ.* **2018**, *130*, 1–13. [CrossRef]
34. Blocken, B. LES over RANS in building simulation for outdoor and indoor applications: A foregone conclusion? *Build. Simul.* **2018**, *11*, 821–870. [CrossRef]
35. Meroney, R.N. Ten questions concerning hybrid computational/physical model simulation of wind flow in the built environment. *Build. Environ.* **2016**, *96*, 12–21. [CrossRef]
36. Zhong, J.; Cai, X.-M.; Bloss, W.J. Modelling the dispersion and transport of reactive pollutants in a deep urban street canyon: Using large-eddy simulation. *Environ. Pollut.* **2015**, *200*, 42–52. [CrossRef] [PubMed]
37. Ashie, Y.; Kono, T. Urban-scale CFD analysis in support of a climate-sensitive design for the Tokyo Bay area. *Int. J. Climatol.* **2011**, *31*, 174–188. [CrossRef]
38. Hang, J.; Wang, Q.; Chen, X.; Sandberg, M.; Zhu, W.; Buccolieri, R.; Di Sabatino, S. City breathability in medium density urban-like geometries evaluated through the pollutant transport rate and the net escape velocity. *Build. Environ.* **2015**, *94*, 166–182. [CrossRef]
39. Zhang, K.; Chen, G.W.; Zhang, Y.; Liu, S.H.; Wang, X.M.; Wang, B.M.; Hang, J. Integrated impacts of turbulent mixing and NOx-O_3 photochemistry on reactive pollutant dispersion and intake fraction in shallow and deep street canyons. *Sci. Total. Environ.* **2020**, *712*, 135553. [CrossRef]
40. Li, Q.; Liang, J.; Wang, Q.; Chen, Y.; Yang, H.; Ling, H.; Luo, Z.; Hang, J. Numerical Investigations of Urban Pollutant Dispersion and Building Intake Fraction with Various 3D Building Configurations and Tree Plantings. *Int. J. Environ. Res. Public Health* **2022**, *19*, 3524. [CrossRef]
41. Padhra, A. *Estimating the Sensitivity of Urban Surface Drag to Building Morphology*; University of Reading: Reading, UK, 2010.
42. Green, S.R. Modelling turbulent air flow in a stand of widely-spaced trees. *Phoenics J.* **1992**, *5*, 294–312.
43. da Costa, J.C.P.L. Atmospheric Flow over Forested and Non-Forested Complex Terrain. Ph.D. Thesis, Universidade do Porto, Porto, Portugal, 2007; pp. 1–159.
44. Santiago, J.L.; Coceal, O.; Martilli, A.; Belcher, S.E. Variation of the sectional drag coefficient of a group of buildings with packing density. *Bound.-Layer Meteorol.* **2008**, *128*, 445–457. [CrossRef]
45. Martilli, A.; Santiago, J.L. CFD simulation of airflow over a regular array of cubes. Part II: Analysis of spatial average properties. *Bound.-Layer Meteorol.* **2007**, *122*, 635–654. [CrossRef]

46. Lien, F.S.; Yee, E. Numerical modelling of the turbulent flow developing within and over a 3-D building array, part I: A high-resolution Reynolds-averaged Navier-Stokes approach. *Bound.-Layer Meteorol.* **2004**, *112*, 427–466. [CrossRef]
47. Sadique, J.; Yang, X.I.A.; Meneveau, C.; Mittal, R. Aerodynamic Properties of Rough Surfaces with High Aspect-Ratio Roughness Elements: Effect of Aspect Ratio and Arrangements. *Bound.-Layer Meteorol.* **2017**, *163*, 203–224. [CrossRef]
48. Oke, T.R. Street Design and Urban Canopy Layer Cliamte. *Energy Build.* **1988**, *11*, 103–113. [CrossRef]
49. Ga, T.; Unger, J.Ã. Detection of ventilation paths using high-resolution roughness parameter mapping in a large urban area. *Build. Environ.* **2009**, *44*, 198–206. [CrossRef]
50. Chen, T.H.; Yang, H.Y.; Chen, G.W.; Lam, C.K.C.; Hang, J.; Wang, X.M.; Liu, Y.L.; Ling, H. Integrated impacts of tree planting and aspect ratios on thermal environment in street canyons by scaled outdoor experiments. *Sci. Total. Environ.* **2021**, *764*, 142920. [CrossRef] [PubMed]
51. Hang, J.; Chen, G.W. Experimental study of urban microclimate on scaled street canyons with various aspect ratios. *Urban Clim.* **2022**, *46*, 101299. [CrossRef]
52. Hang, J.; Wang, D.Y.; Zeng, L.Y.; Ren, L.H.; Shi, Y.R.; Zhang, X.L. Scaled outdoor experimental investigation of thermal environment and surface energy balance in deep and shallow street canyons under various sky conditions. *Build. Environ.* **2022**, *225*, 109618. [CrossRef]
53. Lu, M.R.; Zeng, L.Y.; Li, Q.M.; Hang, J.; Hua, J.J.; Wang, X.M.; Wang, W.W. Quantifying cooling benefits of cool roofs and walls applied in building clusters by scaled outdoor experiments. *Sustain. Cities Soc.* **2023**, *97*, 104741. [CrossRef]